Quaternary Science Reviews 288 (2022) 107579

Contents lists available at ScienceDirect

Quaternary Science Reviews

journal homepage: www.elsevier.com/locate/quascirev

Multiproxy records of temperature, precipitation and vegetation on the central Chinese Loess Plateau over the past 200,000 years

Louise Fuchs [a,*], Bin Zhou [b], Clayton Magill [c,d], Timothy I. Eglinton [c], Youbin Sun [e], Francien Peterse [a,c]

[a] Utrecht University, Department of Earth Sciences, 3584 CS Utrecht, the Netherlands
[b] Nanjing University, School of Earth Sciences and Engineering, Nanjing 210023, China
[c] ETH Zürich, Geological Institute, 8092 Zürich, Switzerland
[d] Lyell Centre, Heriot-Watt University, Edinburgh EH14 7AP, United Kingdom
[e] State Key Laboratory of Loess and Quaternary Geology, Institute of Earth Environment, Chinese Academy of Sciences, Xi'an, 710061, China

ARTICLE INFO

Article history:
Received 3 February 2022
Received in revised form
16 May 2022
Accepted 22 May 2022
Available online 5 June 2022

Handling Editor: Yan Zhao

Keywords:
Paleoclimate
Chinese loess Plateau
Branched GDGTs
Plant waxes
Isotopes
Monsoon

ABSTRACT

The strength of the East Asian Summer Monsoon (EASM) and associated moisture availability have been linked to the spatial distribution of occurrence of C_3 and C_4 vegetation on the Chinese Loess Plateau (CLP). Variations in the stable carbon isotopic composition of organic matter in loess-paleosol sequences from several locations on the CLP indicate that vegetation has shifted from mainly C_3 plants during cool, dry glacials to more C_4 plants during warm, wet interglacials. Although increased temperatures generally lead to an expansion of C_4 vegetation, increased humidity has an opposite effect, as does increasing pCO_2, leaving the exact driver(s) of vegetation change, and thus EASM strength, elusive. Here we reconstruct continuous, directly comparable records of air temperature, monsoon precipitation, and vegetation type over the past 200,000 years based on branched glycerol dialkyl glycerol tetraether (brGDGT) membrane lipids, plant leaf waxes and their isotopic stable carbon and hydrogen isotopic composition ($\delta^{13}C_{wax}$ and δ^2H_{wax}, respectively) preserved at Lingtai on the central CLP. BrGDGT-based temperatures vary between 12 and 21 °C over glacial-interglacial cycles, and consistently lead changes in loess proxies (grain size, magnetic susceptibility), as also observed elsewhere on the CLP. Variations in $\delta^{13}C_{wax}$ are only minor (<2‰) and indicate that C_3 plants have continuously dominated at Lingtai, in contrast to a nearby section where C_4 plants flourished during interglacials. This difference can be explained by the site elevation (~1300 m above sea level), resulting in air temperatures too low for widespread C_4 vegetation occurrence. Instead, variations in the average chain length of the leaf waxes coinciding with large shifts in δ^2H_{wax} (~40‰) during glacial-interglacial transitions suggest that changes in rainfall source and seasonality may have pushed C_3 woody vegetation present during glacials to more non-woody C_3 vegetation during interglacials, as a result of differences in respective water-use efficiency. Our multiproxy records thus indicate that subtle changes in the C_3 species composition can be used to reveal variations in EASM precipitation dynamics in elevated areas where temperature exerts a first order control on the vegetation type.

1. Introduction

The Chinese Loess Plateau (CLP) consists of thick, wind-deposited dust layers. Its position at the margin of the current penetration limit of the East Asian Summer Monsoon (EASM; Fig. 1) marks its sensitivity to (past) climate change. Indeed, the alternating layers of loess and paleosols reflect the sequence of glacial-interglacial cycles, where variations in grain size and magnetic susceptibility throughout multiple sections of the CLP indicate that glacial periods were cool and dry resulting from the position of the Westerlies and the Siberian High, whereas interglacials were warm and wet due to the input of moist air from the warm Pacific Ocean by the summer monsoon (e.g. Porter and An, 1995; An et al., 2000). Our understanding of past EASM dynamics is mostly based on

* Corresponding author. Utrecht University, Department of Earth Sciences, Princetonlaan 6, 3584 CS Utrecht, the Netherlands.
E-mail address: l.fuchs@uu.nl (L. Fuchs).

https://doi.org/10.1016/j.quascirev.2022.107579

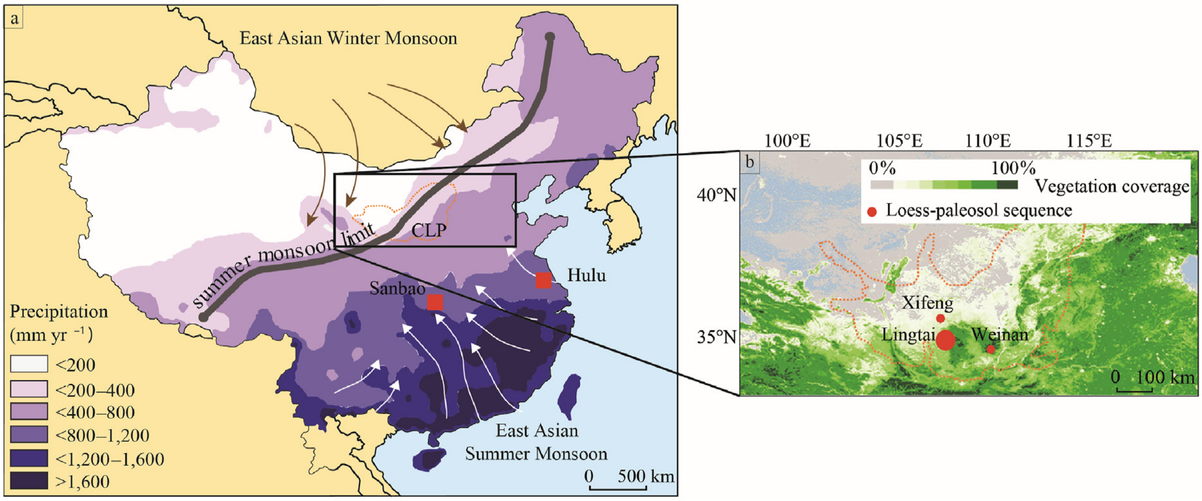

Fig. 1. a) Map indicating the position of the Chinese Loess Plateau (CLP), the location of the Hulu and Sanbao caves, and the average precipitation distribution from 1980–2010 (modified from Blazina et al., 2014). The grey line indicates the northernmost extent of the East Asian Summer Monsoon. White arrows indicate dominant wind directions of the East Asian Summer Monsoon and dark brown arrows indicate dominant wind directions of the East Asian Winter Monsoon; b) Zoomed-in map of the Chinese Loess Plateau (CLP) showing the location of the Lingtai loess-paleosol sequence (this study) and the CLP-sections referred to in the main text. The modern vegetation coverage of the CLP is in the background (modified from Lu et al., 2019). (For interpretation of the references to colour in this figure legend, the reader is referred to the Web version of this article.)

oxygen isotope records ($\delta^{18}O$) from Chinese caves, which follow Northern Hemisphere (NH) July insolation, consequently proposed as a strong control on EASM precipitation dynamics (Wang et al., 2008; Cheng et al., 2016). However, there is an ongoing debate on the interpretation of the speleothem $\delta^{18}O$ record as precipitation intensity (i.e. amount), as the oxygen isotope signal is also influenced by other factors, such as moisture transport path, source, seasonality, and temperature (e.g., Clemens et al., 2010; Pausata et al., 2011; Liu et al., 2015). Modeling approaches suggest that orbital scale variations in the Chinese speleothem $\delta^{18}O$ records are best explained by meridional migration of the Asian monsoon circulation, causing changes in moisture source and rainout (Hu et al., 2019). Past EASM precipitation dynamics have also been studied using the stable isotopic composition of total organic carbon ($\delta^{13}C_{org}$) in loess-paleosol sequences (LPS), as the occurrence of C_3 and C_4 vegetation on the modern CLP relates to the intensity of the EASM (Liu et al., 2005), where intensity refers to both the amount of precipitation as well as the duration of the wet season. Several studies have shown that vegetation changed from mostly C_3 vegetation during glacials, to more C_4 vegetation during interglacials (e.g. Vidic and Montañez, 2004; An et al., 2005; Liu et al., 2005; Yang et al., 2015). However, $\delta^{13}C_{org}$ signals can be affected by preferential degradation of discrete carbon pools or microbial overprinting (e.g. Xie et al., 2004), which can introduce an interpretational bias toward C_4 vegetation in reconstructions using this method, and could thus overestimate the penetration depth and strength of the EASM. In addition, expansion of C_4 vegetation is generally driven by higher temperatures, whereas humidity and pCO_2 that simultaneously increase with temperature during interglacials favor C_3 vegetation (Huang et al., 2001; Rao et al., 2010). This contradiction has not yet been resolved due to an absence of independent paleorecords of air temperature, monsoon precipitation intensity and vegetation type, thereby preventing a mechanistic determination of the spatial evolution of EASM precipitation and thus complicating projections of EASM intensity response to global warming.

Here we use different suites of lipid biomarkers preserved in the loess-paleosol sequence at Lingtai to reconstruct EASM evolution on the central CLP over the past 200,000 years (Fig. 1). Long chain *n*-alkanes are derived from leaf waxes predominantly produced by higher plants to protect against moisture loss (Eglinton and Hamilton, 1967). Leaf waxes stored in sedimentary archives represent an integration of the vegetation signals from a larger area, averaging out plant-to-plant differences (Sachse et al., 2012). Additionally, targeting these compounds ensures a vegetation signal that is unaltered by degradation or microbial overprinting during storage in a sedimentary archive (Eglinton and Logan, 1991; Collister et al., 1994). Although the average chain length (ACL) of *n*-alkanes cannot be related to vegetation type on a global scale, the ACL is often used as a proxy for plant type in paleoclimate reconstructions as the ACL can be linked to environment-changed-induced vegetation changes on a local scale (Bush and McInerney, 2013). The stable carbon isotopic composition ($\delta^{13}C_{wax}$) of long chain *n*-alkanes furthermore provides information on vegetation type due to the different CO_2 fixation pathways used by C_3 and C_4 vegetation causing distinct fractionation patterns (Farquhar et al., 1989; Diefendorf et al., 2010). The isotopic composition of the source water used for lipid synthesis is reflected by their hydrogen isotopic signature (δ^2H_{wax}) and is used to reconstruct precipitation intensity (Sessions et al., 1999; Sachse et al., 2012). Finally, branched glycerol dialkyl glycerol tetraethers (brGDGTs) are membrane lipids of temperature-sensitive bacteria, and are used as a proxy for mean air temperature (MAT) based on their degree of methylation (MBT'_{5ME}; Weijers et al., 2007; De Jonge et al., 2014; Dearing Crampton-Flood et al., 2020). Applied together, these proxies will create a robust framework for a comprehensive assessment of the drivers of (past) vegetation dynamics, and thereby EASM intensity on the central CLP.

2. Materials and methods

2.1. Study site

The Lingtai section is situated in the central part of the CLP at ~1340 m above sea level (35°04′N, 107°39′E, Fig. 1), in the zone where C_3 shrubs and trees that dominate the relatively arid and cool northwestern part of the CLP gradually transition to the C_4 grasses that cover the wetter and warmer southeast (An et al., 2005). Modern monthly air temperature ranges from −5 to 21 °C, with an annual mean of 8.8 °C. Mean annual precipitation amounts to 580 mm, most of which falls between July and September (Zhou et al., 2016).

Lipid biomarkers were analyzed in 10 cm thick layers collected at 0.5 m intervals from the upper 18.5 m of the LPS. The section covers the past 200,000 years based on the correlation of the quartz grain size record from Lingtai (Sun et al., 2006) with the global benthic $\delta^{18}O$ stack (Lisiecki and Raymo, 2005), resulting in an average resolution of our records of ~5 ka between datapoints.

2.2. Lipid biomarker analysis

Biomarkers were extracted (3x) from freeze-dried loess (~20 g) with dichloromethane (DCM): MeOH (9:1, v:v) using an Accelerated Solvent Extractor (ASE, DIONEX 200). A known amount of C_{46} GDGT standard was added to the total lipid extracts (TLEs), after which they were dried under N_2. Subsequently, TLEs were split into an apolar and polar fraction over a 5% water deactivated Si column eluting with hexane:DCM (9:1, v:v) and DCM:MeOH (1:1, v:v), respectively.

The apolar fractions, containing the *n*-alkanes, were analyzed on an Agilent 7890A gas chromatograph equipped with a VF1 column (30 m, 0.25 mm, 0.25 μm) coupled to a flame ionization detector (FID). The carbon and hydrogen isotopic compositions of individual compounds were measured using GC-isotopic ratio mass spectrometry (GC-IRMS; Thermo Trace GC Ultra connected to a Delta V Plus mass IRMS, via an Isolink combustion furnace and ConFlo IV interface). The GC was equipped with a Gerstel CIS-6 PTV GC-inlet set in solvent vent mode, connected to an Agilent VF-1ms column (60 m length x 0.25 mm I.D. x 0.25 μm film thickness). Helium was used as a carrier gas (1 mL/min at constant flow). The GC oven temperature program was as follows: 45 °C (for 1 min) to 130 °C (at 40 °C/min), to 320 °C (at 40 °C/min), at which it was held isothermal for 22.09 min. Reported values are based on at least duplicate analysis of each sample. $\delta^{13}C$ values are expressed in per mille relative to Vienna Pee Dee Belemnite (VPDB) standard and comparison to the A4-mix (A. Schimmelmann, University of Indiana). Standard deviation of the A4-mix over the time of measurement was always <0.4‰. δ^2H values are normalized to Vienna Standard Mean Ocean Water (VSMOW) and comparison with the A5-mix. The H_3^+-factor was determined daily and was 4.2 on average over the measurement period. The average standard deviation of the A5-mix over the time of measurement was 6.5‰ for 6 replicates with varying concentrations.

The polar fraction, containing the GDGTs, was dissolved in hexane:2-propanol (99:1, v/v) and filtered over a 0.45 μm PTFE filter prior to analysis using high performance liquid chromatography-mass spectrometry (HPLC-MS; Agilent 1260 Infinity), with settings according to Hopmans et al. (2016). In short, the GDGTs were separated over two silica Waters Acquity UPLC BEH Hilic columns (1.7 μm, 2.1 mm × 150 mm) at 30 °C preceded by a guard column with the same packing. GDGTs were eluted isocratically at a flow rate of 0.2 mL/min using 82% A and 18% B for 25 min, followed by a linear gradient to 70% A and 30% B for 25 min, where A = hexane and B = hexane: isopropanol (9 : 1, v/v). Injection volume was 10 μL. Ionization of the GDGTs was accomplished using atmospheric pressure chemical ionization with the following source conditions: gas temperature 200 °C, vaporizer temperature 400 °C, drying gas (N_2) flow 6 L/min, capillary voltage 3500 V, nebulizer pressure 25 psi, corona current 5.0 μA. GDGTs were detected and identified by single ion monitoring of the $[M+H]^+$-ions, and quantified by comparing the area of each GDGT peak in the chromatogram to that of the internal standard (cf. Huguet et al., 2006) using Chemstation software B.04.03.

2.3. Proxy calculations

The Average Chain Length (ACL) was calculated for *n*-alkanes C_{27} to C_{33} as follows, where nC_{xx} represents the peak area in the chromatogram:

$$ACL_{27-33} = (27 \times nC_{27} + 29 \times nC_{29} + 31 \times nC_{31} + 33 \times nC_{33}) \\ / \, (nC_{27} + nC_{29} + nC_{31} + nC_{33})$$

Air temperatures were calculated using the MBT'_{5ME} index (De Jonge et al., 2014):

$$MBT'_{5ME} = Ia + Ib + Ic/Ia + Ib + Ic + IIa + IIb + IIc + IIIa$$

and the $BayMBT_0$ model (Dearing Crampton-Flood et al., 2020), using a prior mean of 13.4 °C based on the average modern air temperature for all months >0 °C at Lingtai, and 15.0 °C as a prior standard deviation, generating MAT for months above freezing. The residual mean standard error on the temperature estimates generated with this proxy is 3.8 °C (Dearing Crampton-Flood et al., 2020).

The plant wax stable carbon and hydrogen isotopic compositions are reported as weighted mean of the $C_{29}-C_{33}$ alkanes.

3. Results and discussion

3.1. Glacial-interglacial air temperature variability

BrGDGTs are present throughout the studied interval, and reflect the expected glacial-interglacial temperature variability, with higher MAT during interglacials than during glacials. The temperature estimate of 12.7 °C for the youngest sample (dating ~2 ka BP) matches well with the modern measured MAT for all months >0 °C of ~13 °C at this site. Furthermore, absolute temperature estimates are in the same range as those reconstructed for Xifeng, which has similar climatic conditions and is located about 100 km north of Lingtai (Lu et al., 2019, Fig. 1), and they are on average 7 °C lower than at Weinan and Lantian, situated only ~200 km east of Lingtai but at 700 m lower elevation (Figs. 1 and 3; Thomas et al., 2016; Tang et al., 2017; Lu et al., 2019), explaining the temperature difference and confirming the robustness of our record. At Lingtai, MAT leads magnetic susceptibility (Fig. 2d and e), which represents soil formation and is generally used as a proxy for summer monsoon intensity. This trend is consistent with the decoupling between these parameters also observed elsewhere on the CLP (e.g., Peterse et al., 2011; Gao et al., 2012; Lu et al., 2019). The offset between atmospheric warming and precipitation intensity has been attributed to the direct response of air temperature to solar radiation compared to the intensification of monsoon precipitation, which may have been delayed by the presence of NH ice sheets blocking important atmospheric teleconnections (Peterse et al., 2011, 2014; Thomas et al., 2016). Lu et al. (2019) proposed that the early warming reflected by brGDGTs could alternatively be explained by EASM related changes in the vegetation cover, which would introduce certain climate feedbacks. For example, loess layers deposited during cold and dry conditions with limited vegetation cover would have a more efficient heat adsorption. This would warm the soil and thereby trigger the brGDGTs to record higher-than-expected glacial temperatures (Lu et al., 2019). Regardless of the mechanism, some of the existing brGDGT-based MAT records seem to suggest that warming leads insolation (Fig. 3), which is hard to explain from a physical perspective, and may in part be a consequence of age model uncertainties. Although the chronology of loess sections on the CLP is generally based on the remarkable similarities between loess proxy

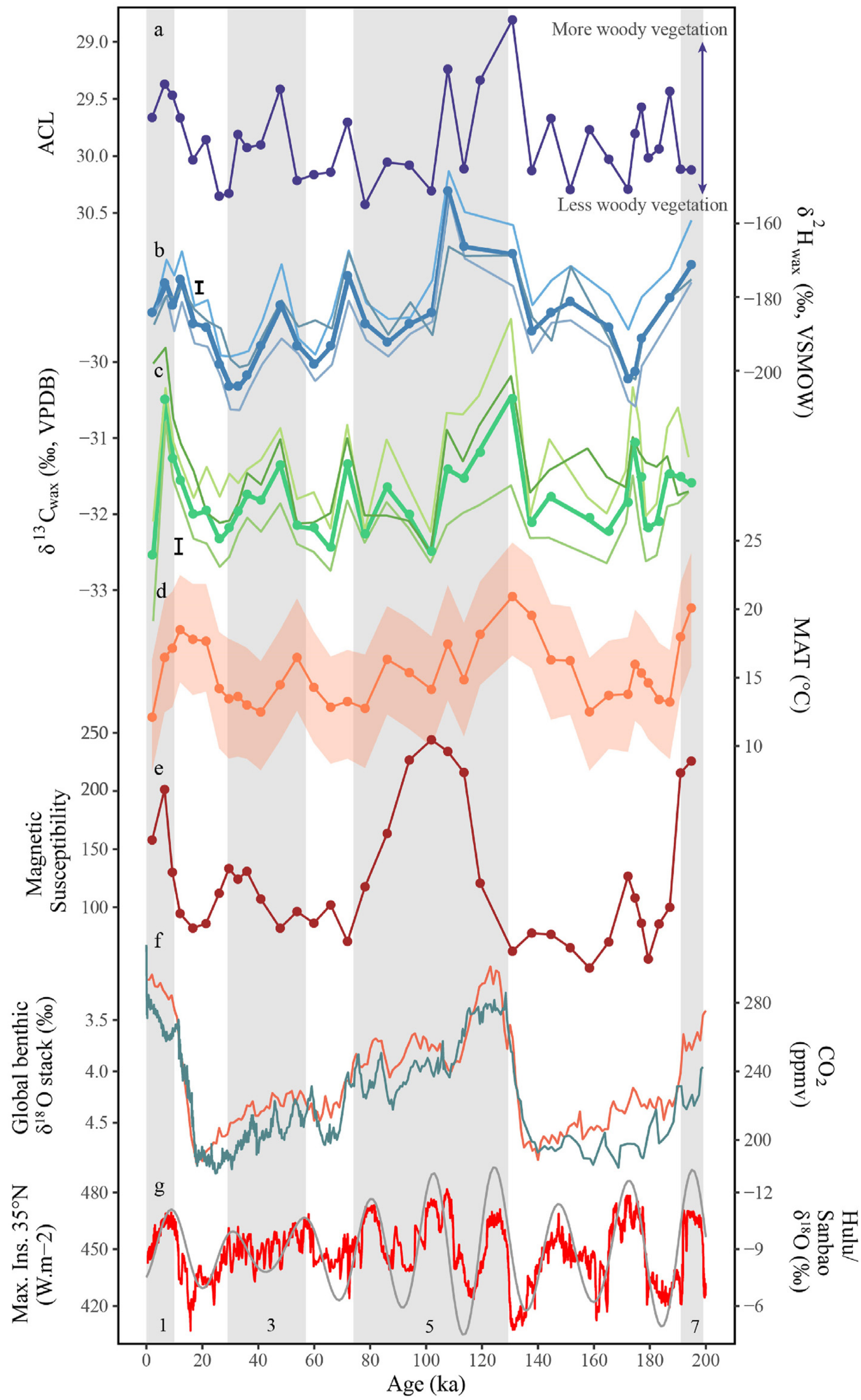

Fig. 2. Comparison of proxy records for the Lingtai LPS. a) Average chain length (ACL) of n-alkanes C_{27-33} representing plant functional type, b) δ^2H_{wax}. Error bar indicates mean standard deviation based on at least duplicate analysis, 1.6‰. VSMOW – Vienna standard mean ocean water. Thick line represents δ^2H_{wax}, thin lines represent δ^2H_{C29}, δ^2H_{C31} and δ^2H_{C33} (light to dark), c) $\delta^{13}C_{wax}$. Error bar indicates standard deviation based on at least duplicate analysis, 0.1‰. VPDB – Vienna Peedee belemnite. Thick line represents $\delta^{13}C_{wax}$, thin lines represent $\delta^{13}C_{C29}$, $\delta^{13}C_{C31}$ and $\delta^{13}C_{C33}$ (light to dark), d) $BayMBT_0$-derived mean air temperature for months > 0°C (MAT). Shaded area indicates the 1σ error on the $BayMBT_0$ record, e) Magnetic susceptibility (Zhou et al., 2016), f) Global benthic $\delta^{18}O$ stack (Lisiecki and Raymo, 2005; orange line) and atmospheric CO_2 concentrations (Bereiter et al., 2012; grey line), g) Composite speleothem $\delta^{18}O$ record from the Hulu (Wang et al., 2001) and Sanbao (Wang et al., 2008) caves (red), and annual maximum insolation at 35°N (grey; Huybers, 2006). Numbers indicate the Marine Isotope Stages (MIS). (For interpretation of the references to colour in this figure legend, the reader is referred to the Web version of this article.)

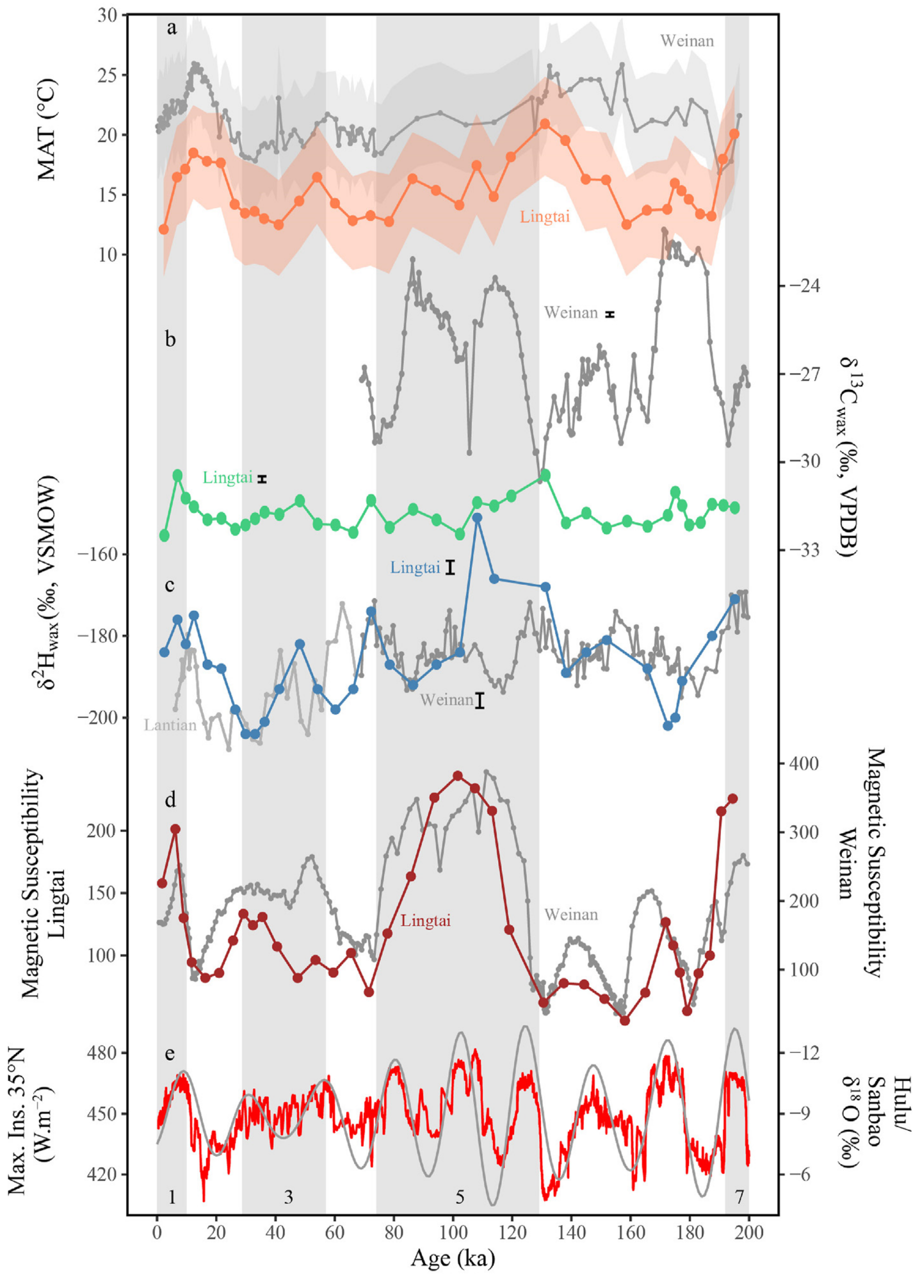

Fig. 3. Comparison of proxy records for the Lingtai LPS and Weinan LPS. a) BayMBT$_0$-derived mean air temperature for months > 0°C (MAT) for Lingtai (this study) and Weinan (recalculated from Tang et al., 2017). Shaded area indicates the 1σ error on the BayMBT$_0$ record, b) $\delta^{13}C_{wax}$. Error bars indicates standard deviation based on at least duplicate analysis, 0.1‰ for Lingtai, 0.1‰ for Weinan (Thomas et al., 2016). VPDB – Vienna Peedee belemnite, c) $\delta^{2}H_{wax}$. Error bar indicates mean standard deviation based on at least duplicate analysis, 1.6‰ for Lingtai, 1.8‰ for Weinan (Thomas et al., 2016). VSMOW – Vienna standard mean ocean water, d) Magnetic susceptibility for Lingtai (Zhou et al., 2016) and Weinan (Tang et al., 2017), e) Composite speleothem $\delta^{18}O$ record from the Hulu (Wang et al., 2001) and Sanbao (Wang et al., 2008) caves (red), and annual maximum insolation at 35°N (grey; Huybers, 2006). Numbers indicate the Marine Isotope Stages (MIS). (For interpretation of the references to colour in this figure legend, the reader is referred to the Web version of this article.)

records (magnetic susceptibility and grain size) and the global benthic stack or speleothem $\delta^{18}O$, this requires the assumption that any changes in the evolution of the EASM were synchronous in time and space (e.g., Porter and An, 1995; Ding et al., 2002; Sun et al., 2021). However, a recent study by Wang et al. (2021) shows that age model tiepoints can shift by±20,000 years when tuning $\delta^{2}H_{wax}$ rather than loess proxy records to speleothem $\delta^{18}O$. As long as this uncertainty in the chronology of loess records is not resolved, the exact timing of deglacial warming in relation to orbital forcing remains uncertain, and leads and lags can only be determined based on (multi-) proxy records obtained from the same section.

3.2. Vegetation changes on the central CLP

Leaf wax *n*-alkanes in the Lingtai LPS show a strong odd-over-even pattern, dominated by C_{29}, C_{31}, and C_{33} *n*-alkanes, with a Carbon Preference Index (CPI) mean of 6.6. Associated $\delta^{13}C_{wax}$ values vary between −30.2‰ and −32.5‰, with the most ^{13}C-enriched homologues in the paleosol layers (Fig. 2c). However, in contrast to magnetic susceptibility, the $\delta^{13}C_{wax}$ record does not tightly parallel glacial-interglacial trends. Furthermore, the range of isotopic variation is relatively small (~2‰), especially when considering that the average $\delta^{13}C_{wax}$ values of C_3 and C_4 plants in modern China are −32‰ and −22‰, respectively (weighed mean for C_{27}, C_{29} and C_{31} *n*-alkanes; Rao et al., 2008). This suggests that C_3 plants have systematically been the dominant vegetation type at Lingtai, unrelated to orbital changes in temperature and pCO_2 over the last 200,000 year (Fig. 2f and g). This is different from the few other $\delta^{13}C_{wax}$ records that exist for the CLP, which show more drastic changes on glacial-interglacial timescales and indicate a substantial increase in C_4 vegetation during interglacials (Zhang et al., 2003, 2006; Liu et al., 2005; Thomas et al., 2016). For example, the $\delta^{13}C_{wax}$ at Weinan is up to 8‰ higher during glacials than during interglacials, indicating a substantial increase in C_4 vegetation under warmer and wetter climte conditions (Fig. 3; Thomas et al., 2016). Since Weinan receives the same amount of annual precipitation as Lingtai, the difference in C_3/C_4 vegetation between these sites is most likely caused by the lower temperature at Ligtai resulting from its elevation, as also suggested earlier by Zhou et al. (2014, using $\delta^{13}C_{pyc}$). Indeed, our brGDGT-based MAT record now confirms that air temperatures at Lingtai were mostly below the suggested threshold of ~15 °C below which C_3 plants have been shown to outcompete C_4 plants at low (<270 ppmv) atmospheric CO_2 levels under modern climate conditions (Huang et al., 2001; Rao et al., 2010). Given that our MAT record represents the average temperature for all months >0 °C, winters were still likely too long and/or harsh for much C_4 vegetation to thrive even during periods when warm season-temperatures exceeded this threshold. This implies that temperature, rather than EASM intensity, should be considered as a first-order control on vegetation type at Lingtai. Regardless, the residual variance in $\delta^{13}C_{wax}$ points at the influence of (an) additional factor(s) on this record.

3.3. Influence of hydroclimate on vegetation type

Past monsoon precipitation in the EAM region is generally inferred from records of speleothem $\delta^{18}O$ and magnetic susceptibility of loess-paleosol sequences (e.g. Porter and An, 1995; Wang et al., 2001), although both these parameters are also influenced by temperature (Wang et al., 2001, 2008). Here we use the stable hydrogen isotopic composition of plant waxes to further unravel past monsoon precipitation dynamics. Records of δ^2H_{wax} are often found to reflect differences in precipitation amount (e.g., Sauer et al., 2001), and could thus also record the alternating wet (depleted δ^2H_{wax}) and dry (enriched δ^2H_{wax}) conditions at the CLP over the glacial-interglacial cycles. Although plant δ^2H_{wax} shows a consistent relation with mean annual precipitation on the modern CLP, differences in hydrogen isotopic fractionation between different vegetation types and its sensitivity to evaporation complicates the translation of δ^2H_{wax} records into quantitative precipitation reconstructions (Liu et al., 2019). At Lingtai, δ^2H_{wax} ranges between −151‰ and −204‰ over the past 200,000 years (Fig. 2b), which is comparable to the range of δ^2H_{wax} in the 130,000 and 350,000 year-long records for the nearby Xifeng and Weinan sections, respectively (Liu and Huang, 2005; Thomas et al., 2016, Fig. 3). Interestingly, like at Weinan, the Lingtai δ^2H_{wax} record shows some of the most depleted values during glacial periods, whereas more enriched values are expected based on the dry conditions prevailing during these intervals, and vice versa. Furthermore, the timing of changes in δ^2H_{wax} does not consistently track the glacial-interglacial transitions indicated by magnetic susceptibility and brGDGT-based MAT (Fig. 2). For the Weinan record, this offset in timing has been attributed to the presence of heterodynes, resulting from the influence of multiple factors operating at different orbital periods on the water isotopes (Thomas et al., 2016). Our Lingtai record has too low resolution to exactly determine the heterodynes, but given the absence of a clear glacial-interglacial trend, we assume that our record thus reflects a mixture of different orbital forcings (i.e., precession, obliquity, and eccentricity). Moreover, the different trends in magnetic susceptibility and δ^2H_{wax} suggests that the amount of monsoon precipitation is decoupled from the isotopic composition of the precipitation on orbital timescales.

To further investigate the trends in δ^2H_{wax} we made a compilation of modern precipitation data (Fig. 4). The data show that meteoric water on the southern CLP is relatively enriched in ^2H during the onset of EASM precipitation in May−June, and becomes more depleted during peak rainfall, reflecting a combined source and amount effect (Fig. 4). The opposite trend is true for the northern CLP, where meteoric water related to the EASM is enriched in ^2H compared to that delivered by the Westerlies during winter. This moisture-source related pattern in water isotopes can result in opposite trends recorded in speleothem and plant wax records (Fig. 2), where EASM precipitation results in an enrichment (depletion) in ^2H on the CLP whilst speleothems are depleted (enriched) in ^{18}O during periods with dominating summer (winter) monsoon (Wang et al., 2001). In addition, (local) recycling of terrestrial precipitation and increased air temperatures may also play a role and will both result in more enriched δ^2H_{wax} values during the warm season (Gat, 1996). Periods with depleted δ^2H_{wax} values (e.g., during MIS3) at Lingtai could thus reflect a moisture source change-induced shift in seasonality, such that vegetation might incorporate a larger contribution of depleted moisture brought in by the Westerlies. At the same time, a transition in precipitation seasonality could cause moisture stress for the prevailing vegetation, prompting a vegetation change in response to moisture limiting conditions (Diefendorf et al., 2010; Ma et al., 2012). A moisture availability-driven vegetation change is supported by our ACL record, which shows a negative correlation with δ^2H_{wax} ($r^2 = 0.28$). The ACL varies between 28.8 and 30.4 (Fig. 2a), in which a low (higher) ACL would then correspond with more (less) woody vegetation (Liu and Huang, 2005).

To further assess the controls on vegetation type at Lingtai, we first evaluate the sources of the individual alkanes by correlating their $\delta^{13}C$ values. We find that the $\delta^{13}C$ values of C_{29} and C_{31} alkanes strongly correlate ($r^2 = 0.73$), but that their relation with the $\delta^{13}C$ of C_{33} alkanes is weak ($r^2 = 0.39$ for C_{29} and $r^2 = 0.20$ for C_{31}), suggesting that C_{33} alkanes are produced by a different vegetation type. Interestingly, the correlations of the δ^2H values of the different alkanes are relatively strong ($r^2 > 0.66$), suggesting that all plant types use a similar moisture source to synthesize their waxes. Nevertheless, the relation between the δ^2H of C_{29} and C_{31} alkanes is stronger ($r^2 = 0.84$) than that between these two alkanes and C_{33} ($r^2 = 0.75$ for C_{31} and $r_2 = 0.65$ for C_{29}), where C_{33} is heavier than would be expected if they would all be produced by the same plant species (Fig. 2). This could mean that C_{33} alkanes are produced by vegetation species that are better adjusted to grow under moisture limited conditions, or that have a different growing season. This scenario would fit with the generally higher ACL during the presumably dry glacial periods in our record (Fig. 2). Although $\delta^{13}C_{wax}$ is only poorly correlated with brGDGT-based MAT ($r^2 = 0.20$), the intrinsic ecological influence of temperature is expressed by the near absence of C_4 vegetation at Lingtai.

Taken together, vegetation type at Lingtai appears to be primarily driven by a temperature threshold (Huang et al., 2001; Zhang et al., 2003; Rao et al., 2010), while the remaining variation can be attributed to changes in plant functional type related to seasonal rainfall distribution. Hence, our multi-proxy records indicate that vegetation at Lingtai shifted between woody and non-woody C_3 vegetation species. In fact, leaf waxes of shrubs on the

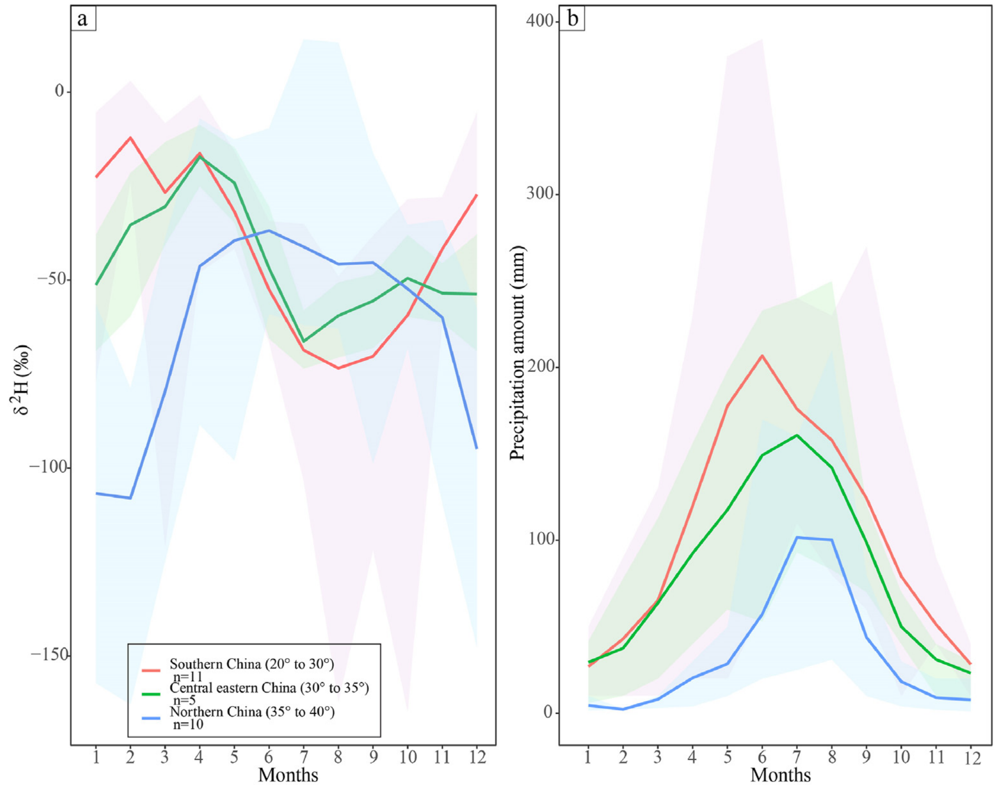

Fig. 4. Monthly precipitation data from meteorological observatories in China (data from IAEA, http://www.univie.ac.at/cartography/project/wiser/), grouped by latitude (Southern China (20° to 30°), Central/Eastern China (30° to 35°), Northern China (35° to 40°)), with n = number of observatories for a) δ^2H, and b) precipitation amount. Thick lines represent the mean value of all stations. The shading represents indicates the maximum range. Lingtai is located at 35°04′N, 107°39′E, at the transition of a predominant amount effect on EASM precipitation δ^2H at latitudes < 35°N and a predominant source effect due to alternating influence of the EASM during summer and the Westerlies during winter at latitudes > 35°N.

modern CLP are enriched in ^{2}H whereas those of grasses are more depleted in ^{2}H (Liu and Huang, 2005), which might have enhanced the variation in the δ^2H_{wax} record. Furthermore, the simultaneous shifts in $\delta^{13}C_{wax}$ and δ^2H_{wax} imply that the timing of changes in vegetation type are linked to transitions from a primarily summer to a more winter monsoon-dominated hydroclimate, or vice versa (Fig. 2b and c).

4. Conclusions

The application of molecular proxies at the Lingtai LPS generated paired records of temperature, precipitation and vegetation type on the central CLP over the past 200,000 years. Although MAT follows the glacial-interglacial variability reflected by magnetic susceptibility, absolute air temperatures were mostly below the threshold for C_4 vegetation to thrive, resulting in a consistent dominance of C_3 vegetation at the site. Instead, vegetation alternated between more/less woody (e.g., trees, shrubs) and non-woody C_3 species (e.g., flowering plants and grasses), likely as a response to moisture stress induced by shifts in the timing of monsoon precipitation during transitions from a more winter to a more summer monsoon dominated hydroclimate. The different variations in δ^2H_{wax} and magnetic susceptibility records indicate that EASM precipitation intensity, reflected by magnetic susceptibility and responding to glacial-interglacial conditions on the CLP, is decoupled from the isotopic composition of moisture used for leaf wax synthesis, recorded by δ^2H_{wax}, which does not follow these cycles. Our multiproxy records indicate that subtle changes in the C_3 species composition can be used to reveal variations in EASM precipitation dynamics in areas where temperature rather than hydroclimate exerts a first order control on the vegetation type. Finally, this study highlights the need for the generation of δ^2H_{wax} records to assess the source(s) and seasonality of EASM precipitation in the geological past.

Author contribution

All authors have read and approved the submitted version of the manuscript, and contributed to this work: Francien Peterse, Bin Zhou, and Timothy I. Eglinton designed the project, Bin Zhou performed fieldwork, Francien Peterse generated the lipid biomarker data, Louise Fuchs, Clayton Magill, Youbin Sun and Francien Peterse interpreted the data, and Louise Fuchs took lead in writing the manuscript. All authors have read and approved the revised version of the manuscript. The manuscript contains original data, and we certify that our data have not been published elsewhere and are also not under consideration for publication elsewhere. All lipid biomarker data used in this study has been submitted to Pangaea (link will be sent when available).

Data availibility statement

Data set for this research is available on Pangea (data submitted, link will be made available when published).

Declaration of competing interest

The authors declare that they have no known competing financial interests or personal relationships that could have appeared to influence the work reported in this paper.

Acknowledgements

We thank Daniel Montluçon (ETH) for assistance with isotope measurements. Klaas Nierop and Jingjing Guo (UU) are thanked for the reanalysis of brGDGTs using the latest chromatography method. This work was financially supported by ETH fellowship FEL-36-11-1 and NWO-Vidi grant no. 192.074 to FP, and carried out under the umbrella of the Netherlands Earth System Science Centre (NESSC). This project has received funding from the European Union's Horizon 2020 research and innovation programme under the Marie Skłodowska-Curie grant agreement No 847504. We would also like to thank the editor and three anonymous reviewers whose feedback greatly improved our manuscript.

References

An, Z., Porter, S.C., Kutzbach, J.E., Xihao, W., Suming, W., Xiaodong, L., Xiaoqiang, L., Weijian, Z., 2000. Asynchronous holocene optimum of the East asian monsoon. Quat. Sci. Rev. 20.

An, Z., Weiguo, L., Zhengtang, G., Clemens, S., Li, L., Prell, W., Youfeng, N., Yanjun, C., Weijian, Z., Benhai, L., Qingle, Z., Yunning, C., Xiaoke, Q., Hong, C., Zhenkun, W., 2005. Multiple expansions of C4 plant biomass in East Asia since 7 Ma coupled with strengthened monsoon circulation. Geology 33, 705. https://doi.org/10.1130/G21423.1.

Bereiter, B., Luthi, D., Siegrist, M., Schupbach, S., Stocker, T.F., Fischer, H., 2012. Mode change of millennial CO2 variability during the last glacial cycle associated with a bipolar marine carbon seesaw. Proc. Natl. Acad. Sci. Unit. States Am. 109, 9755–9760. https://doi.org/10.1073/pnas.1204069109.

Blazina, T., Sun, Y., Voegelin, A., Lenz, M., Berg, M., Winkel, L.H.E., 2014. Terrestrial selenium distribution in China is potentially linked to monsoonal climate. Nat. Commun. 5, 4717. https://doi.org/10.1038/ncomms5717.

Bush, R.T., McInerney, F.A., 2013. Leaf wax n-alkane distributions in and across modern plants: implications for paleoecology and chemotaxonomy. Geochem. Cosmochim. Acta 117, 161–179. https://doi.org/10.1016/j.gca.2013.04.016.

Cheng, H., Edwards, R.L., Sinha, A., Spötl, C., Yi, L., Chen, S., Kelly, M., Kathayat, G., Wang, X., Li, X., Kong, X., Wang, Y., Ning, Y., Zhang, H., 2016. The Asian monsoon over the past 640,000 years and ice age terminations. Nature 534, 640–646. https://doi.org/10.1038/nature18591.

Clemens, S.C., Prell, W.L., Sun, Y., 2010. Orbital-scale timing and mechanisms driving Late Pleistocene Indo-Asian summer monsoons: reinterpreting cave speleothem δ^{18}O: reinterpreting cave speleothem δ^{18}O. Paleoceanography 25. https://doi.org/10.1029/2010PA001926 n/a-n/a.

Collister, J.W., Rieley, G., Stern, B., Eglinton, G., Fry, B., 1994. Compound-specific d13C of leaf lipids from plants with differing carbon dioxide metabolisms. Org. Geochem. 619–627.

De Jonge, C., Hopmans, E.C., Zell, C.I., Kim, J.-H., Schouten, S., Sinninghe Damsté, J.S., 2014. Occurrence and abundance of 6-methyl branched glycerol dialkyl glycerol tetraethers in soils: implications for palaeoclimate reconstruction. Geochem. Cosmochim. Acta 141, 97–112. https://doi.org/10.1016/j.gca.2014.06.013.

Dearing Crampton-Flood, E., Tierney, J.E., Peterse, F., Kirkels, F.M.S.A., Sinninghe Damsté, J.S., 2020. BayMBT: a Bayesian calibration model for branched glycerol dialkyl glycerol tetraethers in soils and peats. Geochem. Cosmochim. Acta 268, 142–159. https://doi.org/10.1016/j.gca.2019.09.043.

Diefendorf, A.F., Mueller, K.E., Wing, S.L., Koch, P.L., Freeman, K.H., 2010. Global patterns in leaf 13C discrimination and implications for studies of past and future climate. Proc. Natl. Acad. Sci. Unit. States Am. 107, 5738–5743. https://doi.org/10.1073/pnas.0910513107.

Ding, Z.L., Derbyshire, E., Yang, S.L., Yu, Z.W., Xiong, S.F., Liu, T.S., 2002. Stacked 2.6-Ma grain size record from the Chinese loess based on five sections and correlation with the deep-sea δ^{18}O record: stacked quaternary climate record from Chinese loess. Paleoceanography 17, 5-1–5-21. https://doi.org/10.1029/2001PA000725.

Eglinton, G., Hamilton, R.J., 1967. Leaf epicuticular waxes. Science 156, 1322–1335. https://doi.org/10.1126/science.156.3780.1322.

Eglinton, G., Logan, G.A., 1991. Molecular preservation. Phil. Trans. Roy. Soc. Lond. B 333, 315–328. https://doi.org/10.1098/rstb.1991.0081.

Farquhar, G.D., Ehleringer, J.R., Hubick, K.T., 1989. Carbon isotope discrimination and photosynthesis. Annu. Rev. Plant Physiol. Plant Mol. Biol. 40, 503–537. https://doi.org/10.1146/annurev.pp.40.060189.002443.

Gao, L., Nie, J., Clemens, S., Liu, W., Sun, J., Zech, R., Huang, Y., 2012. The importance of solar insolation on the temperature variations for the past 110kyr on the Chinese Loess Plateau. Palaeogeogr. Palaeoclimatol. Palaeoecol. 317–318, 128–133. https://doi.org/10.1016/j.palaeo.2011.12.021.

Gat, J.R., 1996. Oxygen and hydrogen isotopes in the hydrologic cycle. Annu. Rev. Earth Planet Sci. 24, 225–262. https://doi.org/10.1146/annurev.earth.24.1.225.

Hopmans, E.C., Schouten, S., Sinninghe Damsté, J.S., 2016. The effect of improved chromatography on GDGT-based palaeoproxies. Org. Geochem. 93, 1–6. https://doi.org/10.1016/j.orggeochem.2015.12.006.

Hu, J., Emile-Geay, J., Tabor, C., Nusbaumer, J., Partin, J., 2019. Deciphering oxygen isotope records from Chinese speleothems with an isotope-enabled climate model. Paleoceanogr. Paleoclimatol. 34, 2098–2112. https://doi.org/10.1029/2019PA003741.

Huang, Y., Street-Perrott, F.A., Metcalfe, S.E., Brenner, M., Moreland, M., Freeman, K.H., 2001. Climate change as the dominant control on glacial-interglacial variations in C3 and C4 plant abundance. Science 293, 1647–1651. https://doi.org/10.1126/science.1060143.

Huguet, C., Hopmans, E.C., Febo-Ayala, W., Thompson, D.H., Sinninghe Damsté, J.S., Schouten, S., 2006. An improved method to determine the absolute abundance of glycerol dibiphytanyl glycerol tetraether lipids. Org. Geochem. 37, 1036–1041. https://doi.org/10.1016/j.orggeochem.2006.05.008.

Huybers, P., 2006. Early pleistocene glacial cycles and the integrated summer insolation forcing. Science 313, 508–511. https://doi.org/10.1126/science.1125249.

Lisiecki, L.E., Raymo, M.E., 2005. A Pliocene-Pleistocene stack of 57 globally distributed benthic δ^{18}O records: pliocene-pleistocene benthic stack. Paleoceanography 20. https://doi.org/10.1029/2004PA001071 n/a-n/a.

Liu, J., Chen, J., Zhang, X., Li, Y., Rao, Z., Chen, F., 2015. Holocene East Asian summer monsoon records in northern China and their inconsistency with Chinese stalagmite δ18O records. Earth Sci. Rev. 148, 194–208. https://doi.org/10.1016/j.earscirev.2015.06.004.

Liu, W., Huang, Y., 2005. Compound specific D/H ratios and molecular distributions of higher plant leaf waxes as novel paleoenvironmental indicators in the Chinese Loess Plateau. Org. Geochem. 36, 851–860. https://doi.org/10.1016/j.orggeochem.2005.01.006.

Liu, W., Huang, Y., An, Z., Clemens, S.C., Li, L., Prell, W.L., Ning, Y., 2005. Summer monsoon intensity controls C4/C3 plant abundance during the last 35 ka in the Chinese Loess Plateau: carbon isotope evidence from bulk organic matter and individual leaf waxes. Palaeogeogr. Palaeoclimatol. Palaeoecol. 220, 243–254. https://doi.org/10.1016/j.palaeo.2005.01.001.

Liu, W., Wang, H., Leng, Q., Liu, H., Zhang, H., Xing, M., Cao, Y., Yang, H., 2019. Hydrogen isotopic compositions along a precipitation gradient of Chinese Loess Plateau: critical roles of precipitation/evaporation and vegetation change as controls for leaf wax δD. Chem. Geol. 528, 119278. https://doi.org/10.1016/j.chemgeo.2019.119278.

Lu, H., Liu, W., Yang, H., Wang, H., Liu, Z., Leng, Q., Sun, Y., Zhou, W., An, Z., 2019. 800-kyr land temperature variations modulated by vegetation changes on Chinese Loess Plateau. Nat. Commun. 10, 1–10. https://doi.org/10.1038/s41467-019-09978-1.

Ma, J.-Y., Sun, W., Liu, X.-N., Chen, F.-H., 2012. Variation in the stable carbon and nitrogen isotope composition of plants and soil along a precipitation gradient in northern China. PLoS One 7, e51894. https://doi.org/10.1371/journal.pone.0051894.

Pausata, F.S.R., Battisti, D.S., Nisancioglu, K.H., Bitz, C.M., 2011. Chinese stalagmite δ18O controlled by changes in the Indian monsoon during a simulated Heinrich event. Nat. Geosci. 4, 474–480. https://doi.org/10.1038/ngeo1169.

Peterse, Francien, Martínez-García, Alfredo, Zhou, Bin, Beets J, Christiaan, Prins A, Maarten, Zheng, Hongbo, Eglinton I, Timothy, 2014. Molecular records of continental air temperature and monsoon precipitation variability in East Asia spanning the past 130,000 years. Quat. Sci. Rev. 83, 76–82. https://doi.org/10.1016/j.quascirev.2013.11.001.

Peterse, F., Prins, M.A., Beets, C.J., Troelstra, S.R., Zheng, H., Gu, Z., Schouten, S., Damsté, J.S.S., 2011. Decoupled warming and monsoon precipitation in East Asia over the last deglaciation. Earth Planet Sci. Lett. 301, 256–264. https://doi.org/10.1016/j.epsl.2010.11.010.

Porter, S.C., An, Z., 1995. Correlation between climate events in the North Atlantic and China during the last glaciation. Nature 375, 305–308.

Rao, Z., Jia, G., Zhu, Z., Wu, Y., Zhang, J., 2008. Comparison of the carbon isotope composition of total organic carbon and long-chain n-alkanes from surface soils in eastern China and their significance. Sci. Bull. 53, 3921–3927. https://doi.org/10.1007/s11434-008-0296-3.

Rao, Z., Zhu, Z., Jia, G., Chen, F., Barton, L., Zhang, J., Qiang, M., 2010. Relationship between climatic conditions and the relative abundance of modern C3 and C4 plants in three regions around the North Pacific. Chin. Sci. Bull. 55, 1931–1936. https://doi.org/10.1007/s11434-010-3101-z.

Sachse, D., Billault, I., Bowen, G.J., Chikaraishi, Y., Dawson, T.E., Feakins, S.J., Freeman, K.H., Magill, C.R., McInerney, F.A., van der Meer, M.T.J., Polissar, P., Robins, R.J., Sachs, J.P., Schmidt, H.-L., Sessions, A.L., White, J.W.C., West, J.B., Kahmen, A., 2012. Molecular paleohydrology: interpreting the hydrogen-isotopic composition of lipid biomarkers from photosynthesizing organisms. Annu. Rev. Earth Planet Sci. 40, 221–249. https://doi.org/10.1146/annurev-earth-042711-105535.

Sauer, P.E., Eglinton, T.I., Hayes, J.M., Schimmelmann, A., Sessions, A.L., 2001. Compound-specific D/H ratios of lipid biomarkers from sediments as a proxy for environmental and climatic conditions. Geochem. Cosmochim. Acta 65, 213–222. https://doi.org/10.1016/S0016-7037(00)00520-2.

Sessions, A.L., Burgoyne, T.W., Schimmelmann, A., Hayes, J.M., 1999. Fractionation of hydrogen isotopes in lipid biosynthesis. Org. Geochem. 30, 1193–1200. https://doi.org/10.1016/S0146-6380(99)00094-7.

Sun, Y., Clemens, S.C., An, Z., Yu, Z., 2006. Astronomical timescale and palaeoclimatic implication of stacked 3.6-Myr monsoon records from the Chinese Loess Plateau. Quat. Sci. Rev. 25, 33–48. https://doi.org/10.1016/j.quascirev.2005.07.005.

Sun, Y., Clemens, S.C., Guo, F., Liu, X., Wang, Y., Yan, Y., Liang, L., 2021. High-sedimentation-rate loess records: a new window into understanding orbital- and millennial-scale monsoon variability. Earth Sci. Rev. 220, 103731. https://

doi.org/10.1016/j.earscirev.2021.103731.

Tang, C., Yang, H., Pancost, R.D., Griffiths, M.L., Xiao, G., Dang, X., Xie, S., 2017. Tropical and high latitude forcing of enhanced megadroughts in Northern China during the last four terminations. Earth Planet Sci. Lett. 479, 98–107. https://doi.org/10.1016/j.epsl.2017.09.012.

Thomas, E.K., Clemens, S.C., Sun, Y., Prell, W.L., Huang, Y., Gao, L., Loomis, S., Chen, G., Liu, Z., 2016. Heterodynes dominate precipitation isotopes in the East Asian monsoon region, reflecting interaction of multiple climate factors. Earth Planet Sci. Lett. 455, 196–206. https://doi.org/10.1016/j.epsl.2016.09.044.

Vidic, N.J., Montañez, I.P., 2004. Climatically driven glacial-interglacial variations in C3 and C4 plant proportions on the Chinese Loess Plateau. Geology 337–340. https://doi.org/10.1130/G20222.1.

Wang, Y., Cheng, H., Edwards, R.L., Kong, X., Shao, X., Chen, S., Wu, J., Jiang, X., Wang, X., An, Z., 2008. Millennial- and orbital-scale changes in the East Asian monsoon over the past 224,000 years. Nature 451, 1090–1093. https://doi.org/10.1038/nature06692.

Wang, Y.J., Cheng, H., Edwards, R.L., An, Z.S., Wu, J.Y., Shen, C.-C., Dorale, J.A., 2001. A high-resolution absolute-dated late pleistocene monsoon record from Hulu cave, China. Science 294, 2345–2348. https://doi.org/10.1126/science.1064618.

Wang, Z., Liu, W., Wang, H., 2021. New chronology of the Chinese loess-paleosol sequence by leaf wax δD records during the past 800 k.y. Geology 49. https://doi.org/10.1130/G48833.1.

Weijers, J.W.H., Schouten, S., van den Donker, J.C., Hopmans, E.C., Sinninghe Damsté, J.S., 2007. Environmental controls on bacterial tetraether membrane lipid distribution in soils. Geochem. Cosmochim. Acta 71, 703–713. https://doi.org/10.1016/j.gca.2006.10.003.

Xie, S., Guo, J., Huang, J., Chen, F., Wang, H., Farrimond, P., 2004. Restricted utility of $\delta^{13}C$ of bulk organic matter as a record of paleovegetation in some loess–Paleosol sequences in the Chinese Loess Plateau. Quat. Res. 62, 86–93. https://doi.org/10.1016/j.yqres.2004.03.004.

Yang, S., Ding, Z., Li, Y., Wang, X., Jiang, W., Huang, X., 2015. Warming-induced northwestward migration of the East Asian monsoon rain belt from the Last Glacial Maximum to the mid-Holocene. Proc. Natl. Acad. Sci. U.S.A. 112, 13178–13183. https://doi.org/10.1073/pnas.1504688112.

Zhang, Z., Zhao, M., Eglinton, G., Lu, H., Huang, C., 2006. Leaf wax lipids as paleovegetational and paleoenvironmental proxies for the Chinese Loess Plateau over the last 170kyr. Quat. Sci. Rev. 25, 575–594. https://doi.org/10.1016/j.quascirev.2005.03.009.

Zhang, Z., Zhao, M., Lu, H., Faiia, A.M., 2003. Lower temperature as the main cause of C4 plant declines during the glacial periods on the Chinese Loess Plateau. Earth Planet Sci. Lett. 214, 467–481. https://doi.org/10.1016/S0012-821X(03)00387-X.

Zhou, B., Shen, C., Sun, W., Bird, M., Ma, W., Taylor, D., Liu, W., Peterse, F., Yi, W., Zheng, H., 2014. Late Pliocene–Pleistocene expansion of C4 vegetation in semiarid East Asia linked to increased burning. Geology 42, 1067–1070. https://doi.org/10.1130/G36110.1.

Zhou, B., Wali, G., Peterse, F., Bird, M.I., 2016. Organic carbon isotope and molecular fossil records of vegetation evolution in central Loess Plateau since 450 kyr. Sci. China Earth Sci. 59, 1206–1215. https://doi.org/10.1007/s11430-016-5276-x.